Development of Benchmark Examples for Quasi-Static Delamination Propagation and Fatigue Growth Predictions

Ronald Krueger

National Institute of Aerospace, Hampton, Virginia

Abstract: The development of benchmark examples for quasi-static delamination propagation and cyclic delamination onset and growth prediction is presented and demonstrated for Abaqus/Standard. The example is based on a finite element model of a Double-Cantilever Beam specimen. The example is independent of the analysis software used and allows the assessment of the automated delamination propagation, onset and growth prediction capabilities in commercial finite element codes based on the virtual crack closure technique (VCCT). First, a quasi-static benchmark example was created for the specimen. Second, based on the static results, benchmark examples for cyclic delamination growth were created. Third, the load-displacement relationship from a propagation analysis and the benchmark results were compared, and good agreement could be achieved by selecting the appropriate input parameters. Fourth, starting from an initially straight front, the delamination was allowed to grow under cyclic loading. The number of cycles to delamination onset and the number of cycles during delamination growth for each growth increment were obtained from the automated analysis and compared to the benchmark examples. Again, good agreement between the results obtained from the growth analysis and the benchmark results could be achieved by selecting the appropriate input parameters. The benchmarking procedure proved valuable by highlighting the issues associated with choosing the input parameters of the particular implementation. Selecting the appropriate input parameters, however, was not straightforward and often required an iterative procedure. Overall the results are encouraging, but further assessment for mixed-mode delamination is required.
Keywords: Composites, Crack Propagation, Delamination, Fatigue, Fracture.

1. Introduction

The virtual crack closure technique (VCCT) (Rybicki and Kanninen, 1977; Krueger, 2004) is widely used for computing energy release rates based on results from finite element analyses and to supply the mode separation required when using a mixed-mode fracture criterion to predict delamination onset or growth. As new methods for analyzing composite delamination are incorporated in finite element codes, the need for benchmarking becomes important since each code requires specific input parameters unique to its implementation. Once the parameters have

been identified, they may then be used with confidence to model delamination growth for more complex configurations.

An approach for assessing the mode I, mode II and mixed-mode I/II, delamination propagation capabilities in commercial finite element codes was recently presented and demonstrated for Abaqus/Standard (Krueger, 2008, 2010, 2011, 2012) as well as MD Nastran™ and Marc™[2] (Orifici and Krueger, 2010). The current paper summarizes the development of benchmark cases based on the Double Cantilever Beam (DCB) specimen, and the creation of examples is shown step-by-step. The creation step is independent of the software used. After creating the benchmark, the approach is demonstrated for the automated analysis in the commercial finite element code Abaqus/Standard. Starting from an initially straight front, the delamination is allowed to grow based on the algorithms implemented into the commercial finite element software. Input control parameters are varied to study the effect on the computed delamination propagation and growth. Results obtained from the automated analysis should closely match the results created manually to obtain the benchmark example.

2. Specimen and Model Description

For the current numerical investigation, the Double Cantilever Beam (DCB), as shown in Figure 1, was chosen. The DCB specimen is used to determine the mode I interlaminar fracture toughness, G_{IC}.
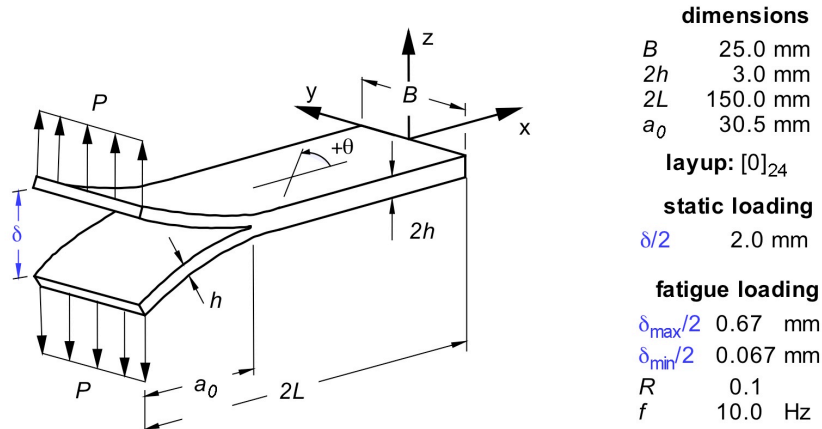

dimensions

B	25.0 mm
$2h$	3.0 mm
$2L$	150.0 mm
a_0	30.5 mm

layup: $[0]_{24}$

static loading

$\delta/2$	2.0 mm

fatigue loading

$\delta_{max}/2$	0.67	mm
$\delta_{min}/2$	0.067	mm
R	0.1	
f	10.0	Hz

Figure 1. Double Cantilever Beam (DCB) Specimen.

Typical two- and three-dimensional finite element models of the DCB specimen are shown in Figures 2 and 3. Along the length, all models were divided into different sections with different mesh refinement. The specimen was modeled with six elements through the specimen thickness. The plane of delamination was modeled as a discrete discontinuity in the center of the specimen.

---

[2] MD Nastran™ and Marc™ are manufactured by MSC.Software Corp., Santa Ana, CA, USA. NASTRAN® is a registered trademark of NASA.

To create the discrete discontinuity, each model was created from separate meshes for the upper and lower part of the specimens with identical nodal point coordinates in the plane of delamination. Two surfaces (top and bottom surface) were created on the meshes as shown in Figure 3. Additionally, a node set was created to identify the intact (bonded nodes) region. The initial delamination front is highlighted in red. The modeling is discussed in detail in related reports (Krueger, 2008, 2010).
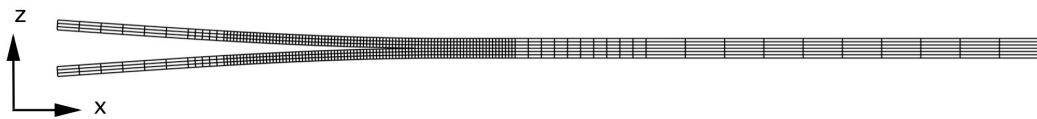

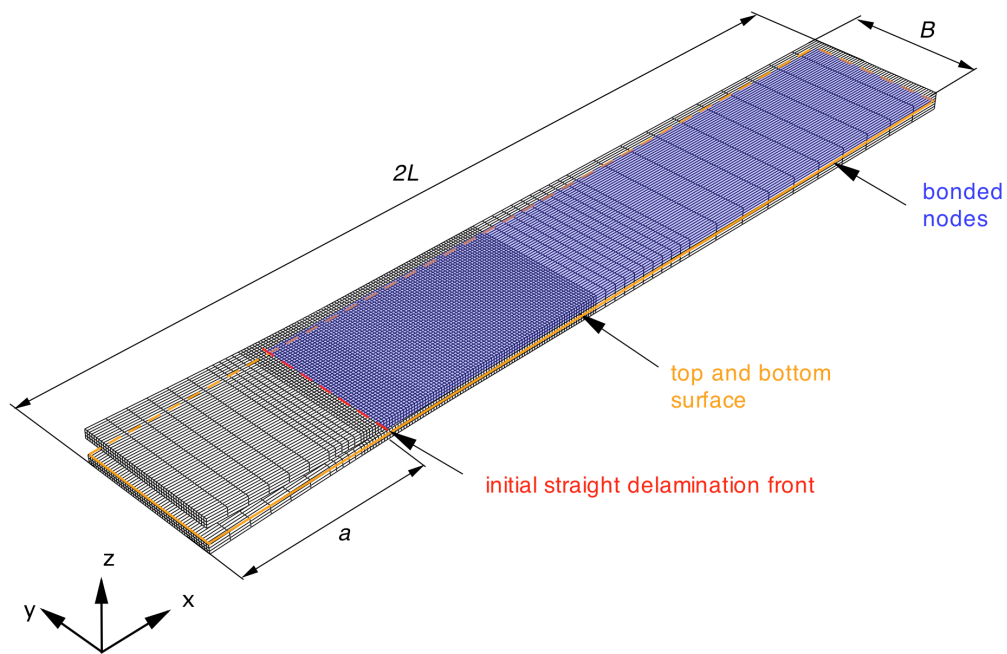**Figure 2. Deformed model of a DCB specimen (plane strain-CPE4).**

Figure 3. Full three-dimensional (solid C3D8I) finite element model of a DCB specimen.

3. Creating a Benchmark Solution for Quasi-Static Loading

First, models simulating specimens with seven different delamination lengths (30 mm ≤ a_0 ≤ 40mm) were analyzed. For each delamination length modeled, the reaction loads P at the location of the applied displacement were calculated and plotted versus the applied opening displacement $\delta/2$ as shown in Figure 4.
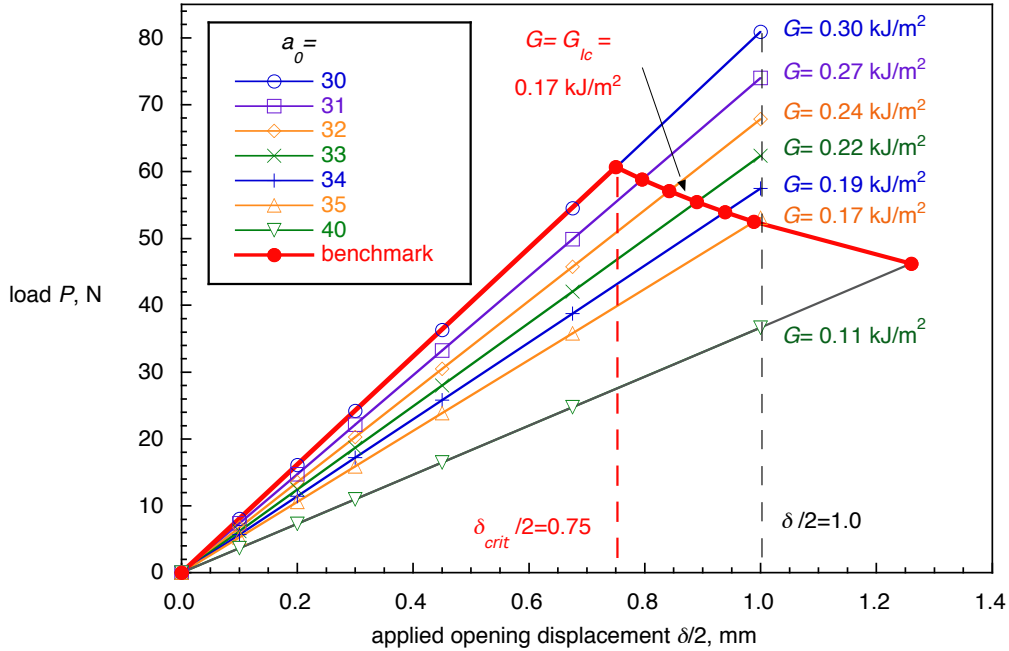

Figure 4. Calculated critical behavior and resulting benchmark case obtained from analyses using three-dimensional models (C3D8I).

The mode I strain energy release rate was calculated along the delamination front across the width of the specimen. The critical load, P_{crit}, when the failure index in the center of the specimen (y/B=0) reaches unity (G_T/G_c=1), can be calculated based on the relationship between load P and the energy release rate.

$$G = \frac{P^2}{2} \cdot \frac{\partial C_P}{\partial A}$$

(1)

In Equation (1), C_P is the compliance of the specimen and ∂A is the increase in surface area corresponding to an incremental increase in load or displacement at fracture. The critical load P_{crit} and critical displacement $\delta_{crit}/2$ were calculated for each delamination length modeled.

$$\frac{G_T}{G_c} = \frac{P^2}{P_{crit}^2} \quad \Rightarrow \quad P_{crit} = P\sqrt{\frac{G_c}{G_T}}, \quad \delta_{crit} = \delta\sqrt{\frac{G_c}{G_T}} \qquad (2)$$

and the results were included in the load/displacement plots as shown in Figure 4 (solid red circles). The results indicate that, with increasing delamination length, less load is required to extend the delamination. This means that the DCB specimen exhibits unstable delamination propagation under load control. Therefore, prescribed opening displacements $\delta/2$ were applied in the analysis instead of nodal point loads P to avoid problems with numerical stability of the analysis. The computed critical load/displacement results were used as a benchmark. The benchmark result may also be visualized by plotting the prescribed opening displacements $\delta/2$ at delamination growth onset versus the delamination length, a, as illustrated in Figure 5. For the delamination propagation, therefore, the load/displacement results obtained from the model of a DCB specimen with an initially straight delamination of a=30 mm length should closely match the critical load/displacement path (solid red line) in Figure 4 or the prescribed opening displacements/delamination-length relationship Figure 5.
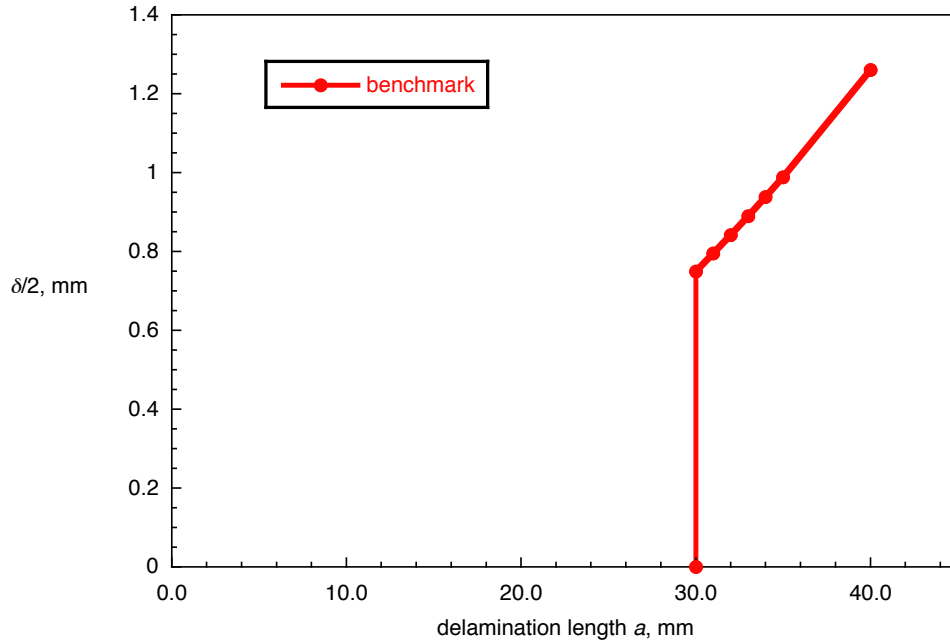

Figure 5. Critical delamination length-displacement behavior for DCB specimen obtained from analyses using three-dimensional models (C3D8I).

4. Results from Automated Propagation Analyses

A set of example results are shown in Figure 6 where the computed resultant force (load P) at the tip of the DCB specimen is plotted versus the applied crack tip opening ($\delta/2$) for different input parameters.
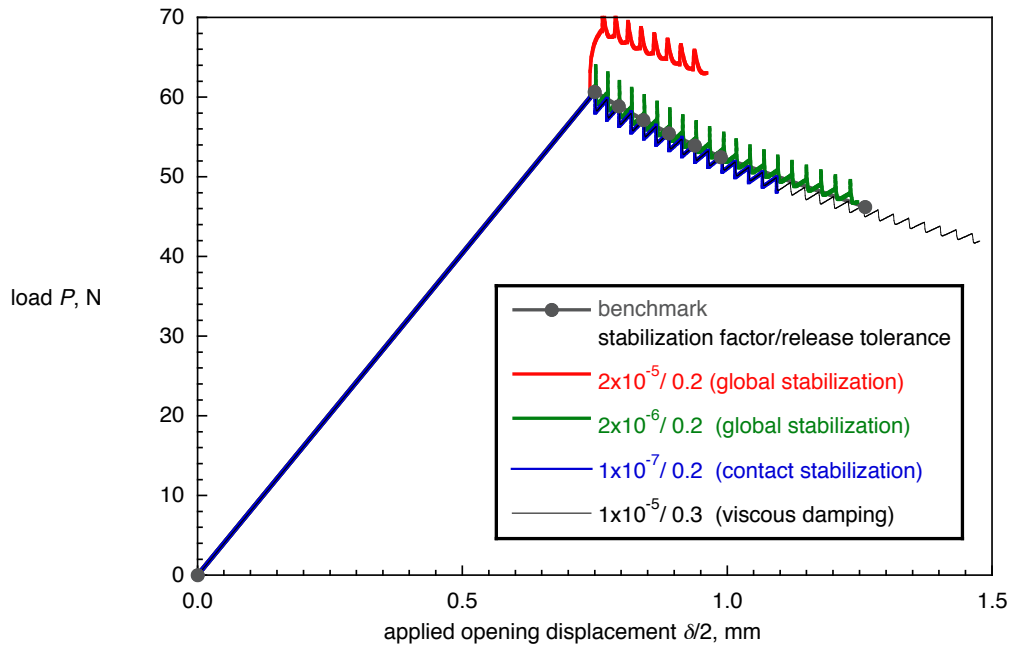

Figure 6. Computed load-displacement behavior obtained from automated analysis using three-dimensional models (C3D8I).

To overcome the convergence problems, the methods implemented in Abaqus/Standard were used individually to study the effects. First, global stabilization was added to the analysis. For a stabilization factor of $2x10^{-5}$, the stiffness changed to almost infinity once the critical load was reached causing the load to increase sharply (plotted in red). The load increased until a point was reached where the delamination propagation started and the load gradually decreased following a saw tooth curve with local rising and declining segments. The gradual load decrease followed the same trend as the benchmark curve (in grey) but is shifted toward higher loads. For a stabilization factor of $2x10^{-6}$ (in green), the same saw tooth pattern was observed but the average curve was in good agreement with the benchmark result. Second, contact stabilization was added to the analysis. For all combinations of stabilization factors and release tolerances, a saw tooth pattern was observed, where the peak values were in good agreement with the benchmark result (example plotted in blue). Third, viscous regularization was added to the analysis to overcome convergence problems. Convergence could not be achieved over a wide range of viscosity coefficients when a default release tolerance value of 0.2 was used. Subsequently, the release

tolerance value was increased. For all combinations of the viscosity coefficient and release tolerance, where convergence was achieved, a saw tooth pattern was obtained, where the peak values were in good agreement with the benchmark result (in black).

An alternative way to plot the benchmark is shown in Figure 7 where the prescribed opening displacements $\delta/2$ at delamination growth onset is plotted versus the delamination length, a, This way of presenting the results is shown, since it may be of advantage for large structures where local delamination propagation may have little influence on the global stiffness of the structure and may therefore not be visible in a global load/displacement plot. However, extracting the delamination length a from the finite element results required more manual, time consuming post-processing of the results compared to the relatively simple and readily available output of nodal displacements and forces. The results plotted in Figure 7 are selected examples that were discussed above. The conclusions that can be drawn from this plot are identical to those discussed above.
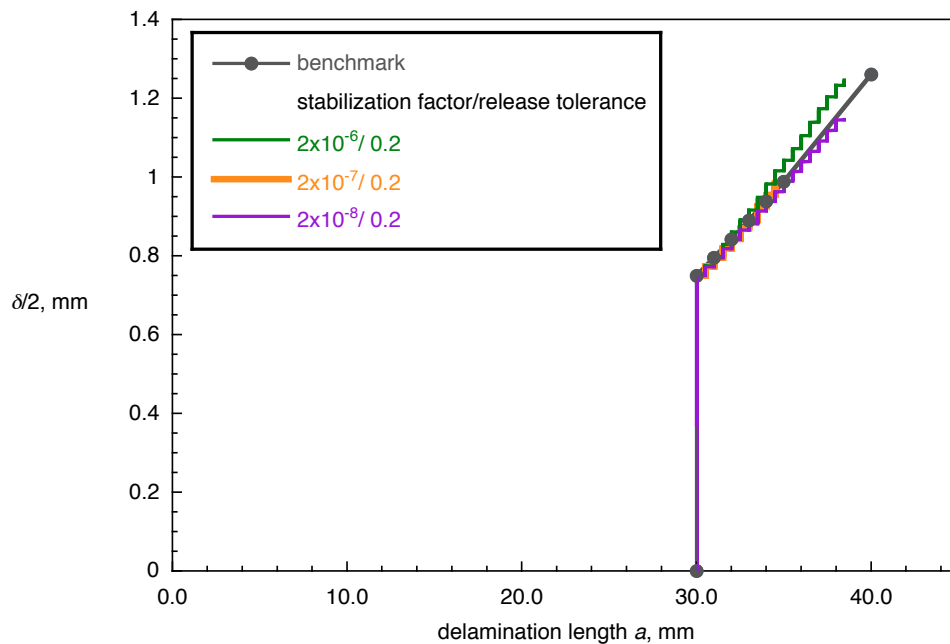

Figure 7. Computed delamination length-displacement behavior obtained from automated analysis using three-dimensional models (C3D8I).

The examples shown highlight the importance of benchmarking to identify critical analysis input parameters. In summary, good agreement between the load-displacement relationship obtained from the propagation analysis results and the benchmark results could be achieved by selecting the appropriate input parameters. However, selecting the appropriate input parameters such as release tolerance, global or contact stabilization and viscous regularization, was not straightforward and often required an iterative procedure. The default setting for global stabilization yielded unsatisfactory results although the analysis converged. The detailed results for Abaqus/Standard

are discussed in detail in a related report (Krueger, 2008). The results of a similar study using the same approach for the finite element codes Marc and MSC.Nastran were published recently (Orifici and Krueger, 2010).

5.   Creating a Benchmark Solution for Cyclic Loading

For the cyclic loading of the specimen, guidance was taken from a draft standard designed to determine mode I fatigue delamination propagation. In the draft document, it is recommended to start the test at a maximum displacement, δ_{max}, which causes the energy release rate at the front, G_{Imax}, to reach initially about 80% of G_{Ic}. For the current study, a critical energy release rate G_{Ic}=0.17 kJ/m^2 was used and the critical values P_{crit} and δ_{crit} (grey dashed lines) were obtained from the benchmark for static delamination propagation shown in the load-displacement plot in Figure 8.
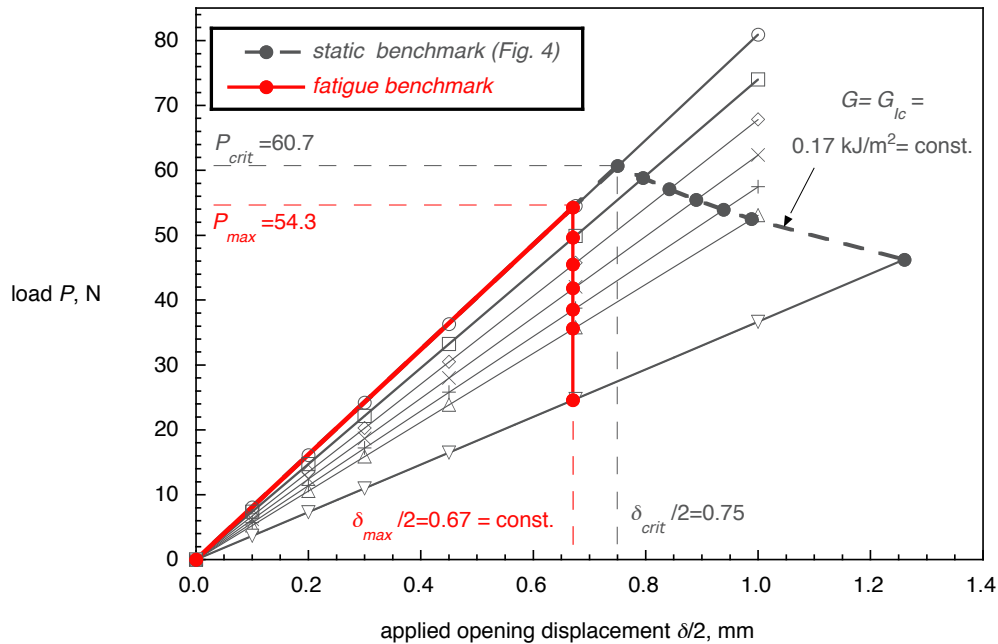

Figure 8. Computed load-displacement behavior obtained from automated analysis using three-dimensional models (C3D8I).

The maximum load, P_{max}, and maximum displacement, $\delta_{max}/2$, were calculated using the known quadratic relationship between energy release rate and applied load or displacement given in Equation (2). The calculated maximum load, P_{max}, and calculated maximum displacement, $\delta_{max}/2$, are shown in Figure 8 (dashed red line) in relationship to the static benchmark case (solid grey circles and dashed grey line) mentioned above. During constant amplitude cyclic loading of a DCB specimen under displacement control, the applied maximum displacement, $\delta_{max}/2$=0.67 mm, is kept constant while the load drops as the delamination length increases (solid red circles and

solid red line). For each of the seven finite element models representing seven delamination lengths (30.0 mm$\leq a_0 \leq$40.0 mm) as shown in Figure 4, the energy release rate corresponding to an applied maximum displacement $\delta_{max}/2$=0.67 mm was calculated using Equation (2). The energy release rate decreases with increasing delamination length, a, as shown in Figure 9 (solid red circles and solid red line). Delamination growth was assumed to stop once the calculated energy release rate drops below the cutoff value, G_{th}, (green solid horizontal line). The static benchmark case (solid grey circles and dashed grey line in Figure 9), where the delamination propagates at constant G_{Ic} (solid blue line in Figure 9) was included for comparison.
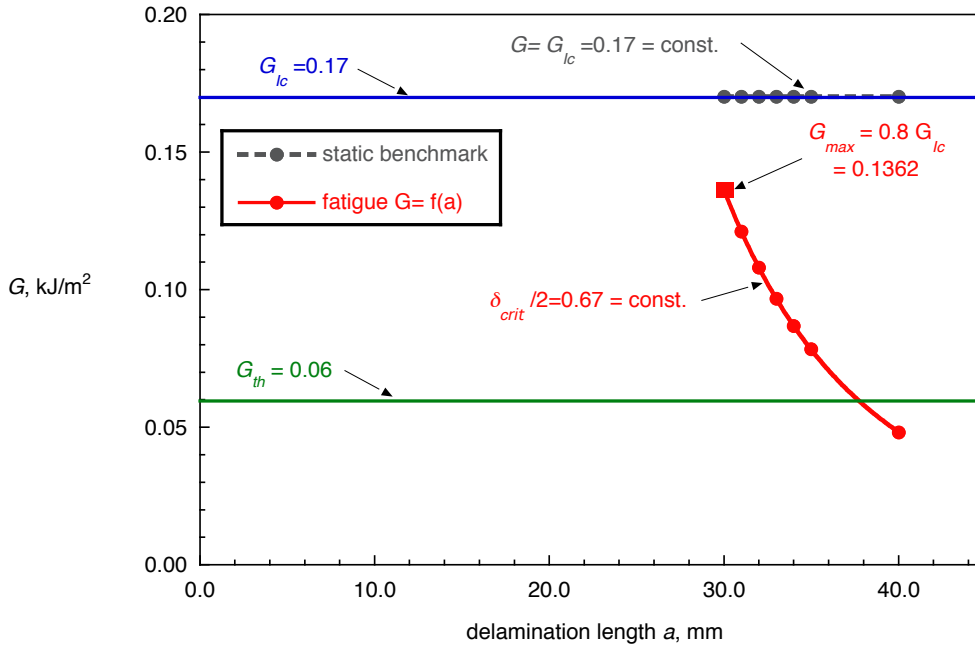

Figure 9. Energy release rate – delamination length behavior for a DCB specimen obtained from two-dimensional models (CPE4).

The number of cycles to delamination onset, N_D, can be obtained from the delamination onset curve which is a power law fit of experimental data obtained from a DCB test using the respective standard for delamination growth onset as shown in Figure 10. Solving for N_D yields

$$G = m_0 \cdot N_D^{m_1} \;\Rightarrow\; N_D = \underbrace{\left(\frac{1}{m_0}\right)^{\frac{1}{m_1}}}_{c_1} \cdot G^{\frac{1}{m_1}} \;\Rightarrow\; N_D = c_1 \cdot G^{c_2}, \quad c_2 = \frac{1}{m_1} \tag{3}$$

At the beginning of the test, the specimen is loaded initially so that the energy release rate at the front, G_{Imax}, reaches about 80% of G_{Ic} corresponding to G_{Imax}=0.1362 kJ/m^2. From the delamination onset curve, the number of cycles to delamination onset is determined as, N_D=150. Details are discussed in a related report (Krueger, 2010).
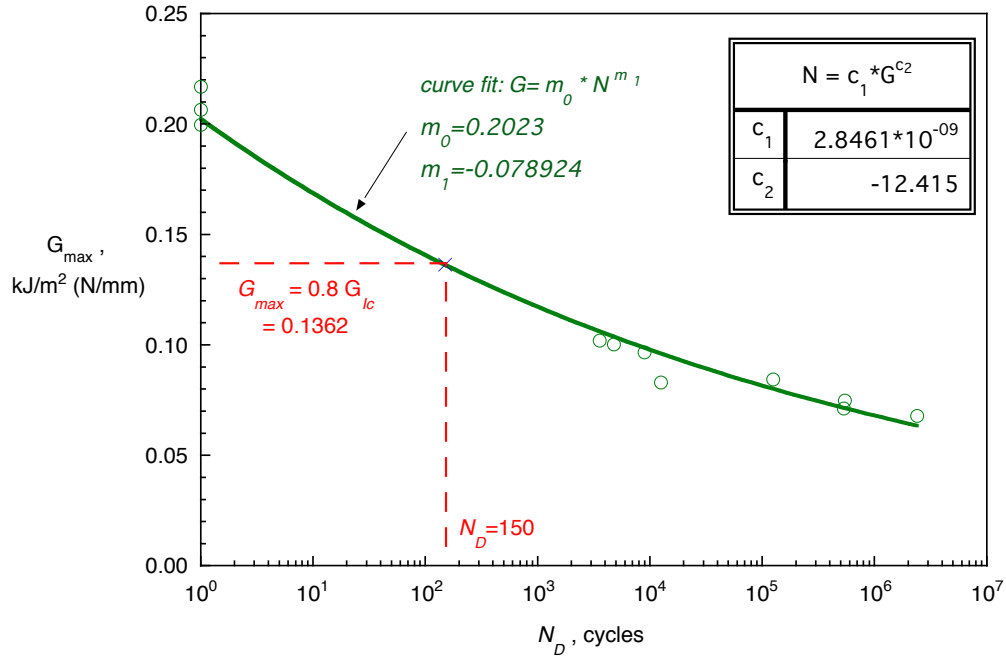
Figure 10. Experimentally determined delamination growth onset for DCB specimen.

The number of cycles during stable delamination growth, N_G, can be obtained from the fatigue delamination propagation relationship (Paris Law) as shown in Figure 11. The delamination growth rate (solid purple line) can be expressed as a power law function

$$\frac{da}{dN} = c \cdot G_{max}^n \qquad \text{or} \qquad \frac{\Delta a}{\Delta N} = c \cdot G_{max}^n \qquad (4)$$

where da/dN is the increase in delamination length per cycle and G_{max} is the maximum energy release rate at the front at peak loading. The factor c and exponent n are obtained by fitting the curve to the experimental data obtained from DCB tests. A cutoff value, G_{th}, was chosen below which delamination growth was assumed to stop. Details are discussed in a related report (Krueger, 2010). Note, that this benchmarking exercise ignores branching, or fiber bridging. Hence, the Paris Law was not normalized with the static R-curve as recently suggested (Krueger, 2010).

For the current study, increments of $\Delta a=0.1$ mm were chosen. Starting at the initial delamination length $a_0=30.5$ mm, the energy release rates $G_{i,max}$ were obtained for each increment, i, from the curve fit (solid red circles and solid red line) plotted in Figure 9. These energy release rate values were then used to obtain the increase in delamination length per cycle or growth rate $\Delta a/\Delta N$ from the Paris Law. The number of cycles during stable delamination growth, N_G, was calculated by summing the increments ΔN_i

$$N_G = \sum_{i=1}^{k} \Delta N_i = \sum_{i=1}^{k} \frac{1}{c} G_{i,max}^{-n} \cdot \Delta a \implies a = a_0 + \sum_{i=1}^{k} \Delta a = a_0 + k \cdot \Delta a \tag{5}$$

where k is the number of increments. The resulting delamination length, a, was calculated by adding the incremental lengths Δa to the initial length a_0.
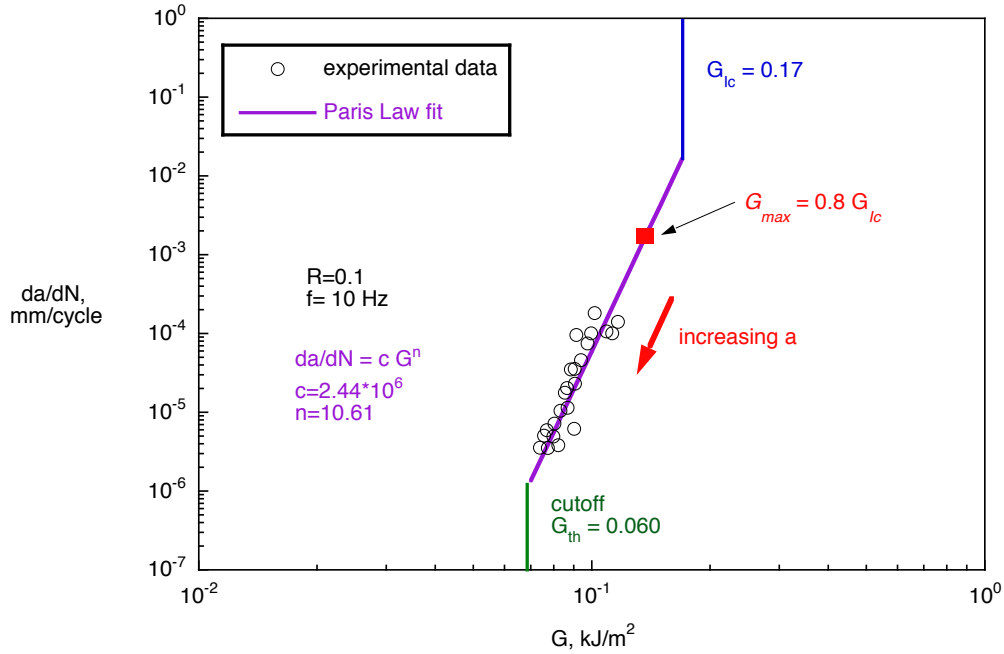

Figure 11. Experimentally determined delamination growth rate (Paris Law).

For the combined case of delamination onset and growth, the total life, N_T, may be expressed as $N_T = N_D + N_G$ where, N_D, is the number of cycles to delamination onset and N_G, is the number of cycles during delamination growth. For this combined case, the delamination length, a, is plotted in Figure 12 for an increasing number of load cycles N_T. For the first N_D cycles, the delamination length remains constant (horizontal red line), followed by a growth section where — over N_G cycles - the delamination length increases following the Paris Law (crosses and solid red line). Once a delamination length is reached where the energy release rate drops below the assumed cutoff value, G_{th}, (as shown in Figure 7), the delamination growth no longer follows the Paris Law (dashed grey line) and stops (horizontal solid red line). A delamination length prediction analysis that accounts for delamination fatigue onset as well as stable growth should yield results that closely resemble the plot in Figure 12. The curve fit (solid red line) can therefore be used as a benchmark.
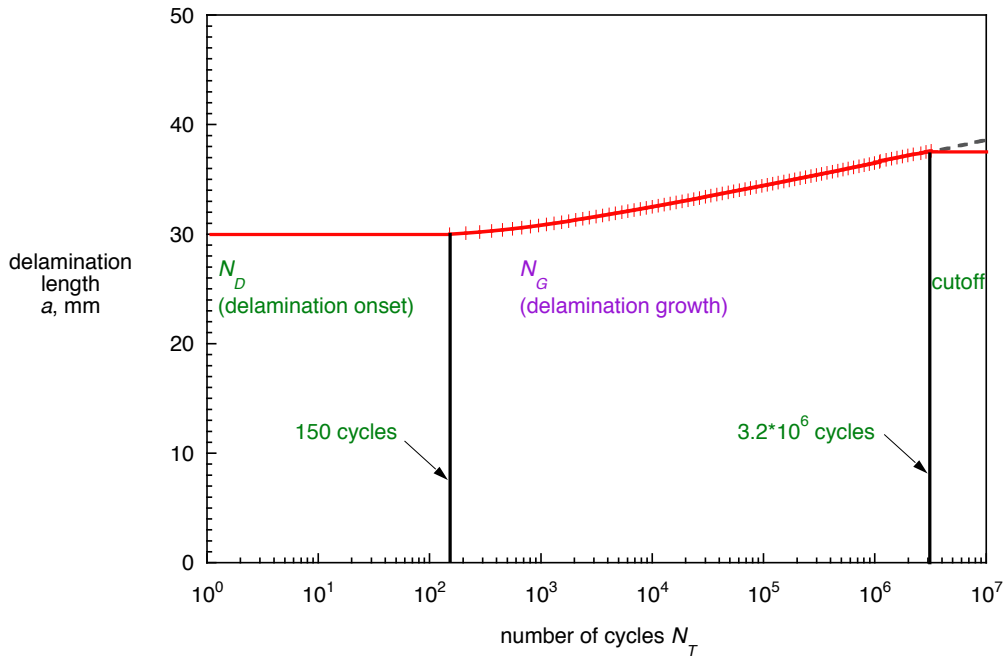
Figure 12. Delamination onset and growth behavior for a DCB specimen obtained from two-dimensional models (CPE4).

6.   Results from Automated Growth Analyses

A set of example results are shown in Figure 13 where the delamination length, a, is plotted versus the number of cycles, N, for different input parameters and models. For all results shown, the analysis stopped when a 10,000,000 cycles limit - used as input to terminate the analysis - was reached.

First, the effect of the initial time increment used in the analysis settings was studied as shown in Figure 13. The initial time increment was varied between i_0=0.01 (one tenth of a single loading cycle, t_s=0.1s, open blue circles and solid blue line) and i_0=0.0001 (one thousandth of a single loading cycle, open green diamonds and solid green line). For larger initial time increments, the onset of delamination shifted towards a lower number of cycles. Reducing the initial time increments, however, significantly increased the computation time. Based on the results, it was therefore decided to use an initial time increment of i_0=0.001 (open red squares and solid red line) for the remainder of the study to save computation time. This step is justified by the fact that the results obtained for i_0=0.001 were almost identical to the values obtained from the analysis where a smaller initial time increment was used (i_0=0.0001). Second, the release tolerance was varied. In the current study, varying the input between 0.2 (the default value) and 0.01 did not have any effect on the computed onset and growth behavior during the analysis. It is assumed that the release tolerance only affects static delamination propagation and not growth under cyclic loading studied here. Stabilization (to overcome the convergence problems) which was required for the

automated delamination propagation under static loading, was not required for automated growth analysis under cyclic loading. However input parameters to define the cyclic loading were varied and showed different affects on the computed results. Also, solution controls had to be manipulated to achieve reasonable computation times. The results from these studies are discussed in detail in a related report (Krueger, 2010).
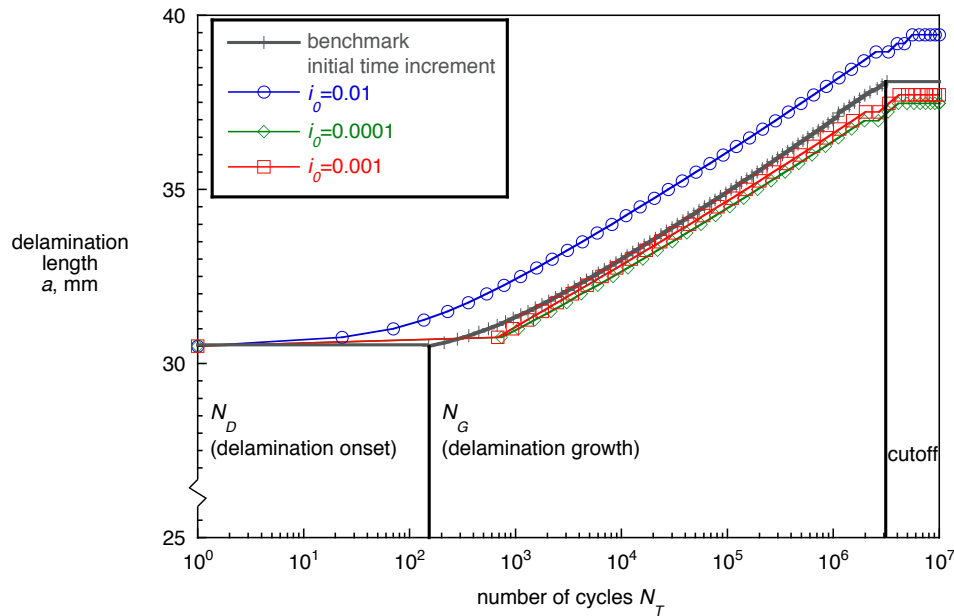

Figure 13. Computed delamination onset and growth obtained from two-dimensional models (CPE4) for different initial time increments i_0.

7. Conclusions

The development of two benchmark examples for static delamination propagation and cyclic delamination growth prediction were presented and demonstrated for the commercial finite element code Abaqus/Standard. The example was based on a finite element model of a Double Cantilever Beam (DCB) specimen, which is independent of the analysis software used and allows the assessment of the delamination propagation and growth prediction capabilities in commercial finite element codes. The development of the benchmark examples was presented step by step. Starting from an initially straight front, the delamination was then allowed to propagate or grow under cyclic loading using automated analyses.

With respect to benchmarking, the results showed the following:

- Benchmark examples for the assessment of automated delamination propagation and growth capabilities can easily be developed from a set of static analyses of models with different initial delamination lengths.

- The development of benchmark examples is independent of the software used and independent of experimental results.
- The benchmarking process can be used to identify the issues associated with the input of a particular finite element code or implementation.
- Benchmarking helps identify relevant input parameters so that they may be used with confidence when modeling more complex configurations.

In general, good agreement between the results obtained from the propagation and growth analysis and the benchmark results could be achieved by selecting the appropriate input parameters. Overall, the results are promising. In a real case scenario, however, where the results are unknown, obtaining the right solution will remain challenging. Further studies are required which should include the assessment of the propagation capabilities in more complex mixed-mode specimens and on a structural level.

8. References

1. Krueger, R., "Virtual Crack Closure Technique: History, Approach and Applications," Applied Mechanics Reviews, (57), pp. 109-143, 2004.
2. Krueger, R., "An Approach to Assess Delamination Propagation Simulation Capabilities in Commercial Finite Element Codes," NASA/TM-2008-215123, 2008.
3. Krueger, R., "Development of a Benchmark Example for Delamination Fatigue Growth Prediction," NASA/CR-2010-216723, NIA report no. 2010-04, 2010.
4. Krueger, R., "Development and Application of Benchmark Examples for Mode II Static Delamination Propagation and Fatigue Growth Predictions," NASA/CR-2011-217305, NIA report no. 2011-02, 2011.
5. Krueger, R., "Development and Application of Benchmark Examples for Mixed-Mode I/II Quasi-Static Delamination Propagation Predictions," NIA report no. 2012-01, 2012.
6. Orifici, A.C. and Krueger, R., "Assessment of Static Delamination Propagation Capabilities in Commercial Finite Element Codes Using Benchmark Analysis," NASA/CR-2010-216709, NIA report no. 2010-03, 2010.
7. Rybicki E.F. and Kanninen, M.F., "A Finite Element Calculation of Stress Intensity Factors by a Modified Crack Closure Integral," Engineering Fracture Mechanics, (9), pp. 931-938, 1977.

9. Acknowledgements